Large-Scale Circulation with Locally Enhanced Vertical Mixing*

R. M. SAMELSON

Woods Hole Oceanographic Institution, Woods Hole, Massachusetts

(Manuscript received 15 October 1996, in final form 6 August 1997)

ABSTRACT

The influence of localized regions of intensified vertical mixing on the stratification and circulation in a large-scale ocean model is investigated with idealized numerical experiments. Numerical solutions are obtained of a closed-basin, single-hemisphere ocean model based on the planetary geostrophic equations. Mesoscale eddy effects are minimized, and vertical mixing at the turbulent microscale is represented by a vertical diffusivity κ_v. Solutions with uniform κ_v are contrasted with a ''localized mixing'' solution, in which κ_v increases by two orders of magnitude from its interior value (0.2×10^{-4} m^2 s^{-1}) in a region 500 km wide adjacent to the vertical eastern boundary. When κ_v is uniform, the stratification beneath the ventilated thermocline is characterized by a single vertical scale. In contrast, the localized vertical mixing supports a deep diffusive thermocline with two distinct vertical scales: an internal boundary layer centered at the base of the ventilated thermocline (roughly 1000-m depth) and an abyssal thermocline whose vertical scale is set in the region of large κ_v. This stratification is qualitatively similar to observed deep ocean stratification. In contrast to the Stommel–Arons meridional abyssal flow that arises in the model when κ_v is uniform and small, the localized mixing solution has primarily zonal flow in the abyssal interior, with meridional motion confined to boundary layers. An advective–diffusive balance is established in the region of enhanced mixing. The near-surface circulation is dominated by westward zonal flow in the southern half of the interior, northward flow along the western boundary, and eastward flow in the northern half of the interior, while the pattern of flow in the abyssal interior is essentially the reverse. The circulation is closed by upwelling in the mixing region and downwelling along the northern boundary. Meridional motion in the mixing region is consistent with the Sverdrup vorticity balance, with northward flow at depth and southward flow near the surface. The source water for the deep circulation is confined to a narrow range of the coldest temperature classes in the basin, while the middepth subtropical thermocline is filled with warmer deep water that enters the gyre as cold deep water and then is modified in the eastern mixing region.

1. Introduction

The discrepancy between diapycnal mixing rates inferred from large-scale budgets (Munk 1966; Hogg 1987) and those inferred from turbulent microstructure measurements (Gregg 1987) and tracer injection experiments (Ledwell et al. 1993) is an intriguing and important paradox in large-scale physical oceanography. These mixing rates are typically quantified in terms of a vertical eddy diffusivity of density, κ_v, for which large-scale budgets indicate values of order 10^{-4} m s^{-2}, while ''direct'' measurements indicate values of order 10^{-5} m s^{-2}. There are many possible resolutions of this paradox. One such possibility is that much of the mixing inferred from large-scale budgets occurs in spatially localized regions (''hot spots''), perhaps along boundaries,

that have been sampled poorly or not at all by the direct measurements. Recent observational evidence for intensified mixing near rough topography in the deep ocean is consistent with this notion (Polzin et al. 1997), though it is not yet clear whether the observed mixing is sufficient to close the relevant budgets; de Szoeke (1995) suggests that even diffusivities of order 10^{-4} m s^{-2} may be insufficiently large.

Motivated in part by the direct measurements of small interior κ_v and following previous work by Colin de Verdiere (1988, 1989) and Salmon (1990), Samelson and Vallis (1997b) have recently analyzed the structure of the subtropical thermocline that arises in numerical solutions of a closed-basin, single-hemisphere, planetary geostrophic circulation model when κ_v is of order 10^{-5} m s^{-2}. They find that for these small values of κ_v, the subtropical thermocline is composed of two distinct components, an adiabatic ''ventilated'' thermocline (Luyten et al. 1983) near the surface and an intrinsically diffusive ''internal boundary layer'' thermocline (Salmon 1990) at the base of the wind-driven motion. Downward diffusion of heat through the internal boundary layer is balanced by upwelling of dense abyssal fluid that is in turn supplied from a convectively adjusting

subpolar gyre by a geostrophic deep western boundary current, roughly in accord with the theory of Stommel and Arons (1960). The internal boundary layer collapses toward a discontinuity as κ_v is reduced toward zero, as there is no mechanism to force heat downward beneath the ventilated thermocline. Consequently, for these small values of κ_v, the abyssal fluid is much more homogeneous, and the deep stratification much weaker, in the model than in the ocean. A similar effect has been observed in primitive equation basin models (Cummins 1991). This suggests that fundamental elements of the abyssal circulation are not represented in the model. One such element may be enhanced turbulent mixing that may occur in restricted areas, for example, near boundaries. In this regard, the departure of the abyssal stratification in the model from the observed structure of the deep ocean can be seen as a dynamical counterpart of the discrepancy between the observed estimates of vertical mixing from large-scale budgets and direct measurements.

The present idealized numerical experiments are intended to give a preliminary appreciation of the influence that localized regions of intensified vertical mixing can have on the stratification in the large-scale ocean circulation model developed by Samelson and Vallis (1997a,b). They are not intended to resolve the question of whether these processes are dominant in the abyssal ocean. Rather, the model is intended to serve as a simple and relatively accessible context in which the general properties of their effects might be explored. In the main experiment, the vertical diffusivity is increased by two orders of magnitude in a region adjacent to the eastern boundary. This calculation is one of a set of similar calculations with spatially varying vertical diffusivity that has been conducted with various versions of the planetary geostrophic model. It illustrates, in a particularly clear way, a number of characteristic features found in many of the others. A comprehensive synthesis and analysis will not be attempted here. The present results complement those of Cummins (1991), who showed that a depth-dependent, but horizontally uniform, vertical diffusivity could reproduce observed mean deep stratification in a primitive equation model.

2. Model formulation

The basic model is the planetary geostrophic circulation model described by Samelson and Vallis (1997a,b). It consists of an interior domain with nearly geostrophic flow capped by a surface boundary layer of fixed depth containing the frictionally driven Ekman flow. The model equations are supplemented by a convective adjustment scheme to prevent the development of static instabilities. For the present calculations, a spatial dependence of the vertical diffusivity is introduced. The equations are summarized below.

a. Interior equations

The interior equations are the hydrostatic–biharmonic diffusive planetary geostrophic equations described by Samelson and Vallis (1997a,b):

$$-fv + p_x = -\varepsilon u \qquad (2.1)$$

$$fu + p_y = -\varepsilon v \qquad (2.2)$$

$$p_z - T = 0 \qquad (2.3)$$

$$u_x + v_y + w_z = 0 \qquad (2.4)$$

$$T_t + uT_x + vT_y + wT_z - \kappa_v T_{zz} = \kappa_h \Delta_h T - \lambda \Delta_h^2 T. \qquad (2.5)$$

Here (u, v, w) are the (x, y, z) components of velocity, t is time, p is pressure divided by a constant reference density ρ_0, T is temperature (with density $\rho = -T$), and subscripts x, y, z, and t denote partial derivatives. These equations admit boundary conditions on normal flow and normal heat flux at each rigid boundary. The Coriolis parameter f is a linear function of y,

$$f = f_0 + \beta(y - y_0), \qquad (2.6)$$

where β, f_0, and y_0 are constants. For the calculations described below, the horizontal diffusivities κ_h, λ and the frictional parameter ε are positive constants, with $\lambda = \lambda_0 = (\varepsilon/\beta)^2 \kappa_h$ to minimize horizontal diffusive fluxes across the tilted isotherms of the western boundary current, as suggested by Samelson and Vallis (1997a). The vertical diffusivity κ_v may be a function of the zonal coordinate x (section 2c). Cartesian coordinates are used for simplicity, and effects of salinity are neglected. The domain has lateral boundaries at $x = \{0, 1\}$ and $y = \{0, 1\}$, and a flat bottom at $z = 0$. The upper boundary of the interior domain at $z = 1$ is the base of the surface boundary layer. The equations are supplemented by a convective adjustment scheme, which removes static instabilities at each time step by vertically mixing grid-point fluid volumes to restore neutral stability.

The upper boundary condition on temperature for the interior equations is obtained from a simple "slab" model of a frictional surface boundary layer with fixed depth $\delta_E \ll 1$ (so the sea surface is at $z = 1 + \delta_E$). The surface boundary layer temperature T_E is obtained from a vertically integrated thermodynamic equation,

$$T_{Et} + (u_A T_E)_x + (v_A T_E)_y = (F_T - F_i)/\delta_E, \qquad (2.7)$$

where F_T is the air–sea flux, F_i is the flux through the base of the boundary layer, and the interior velocity at the base of the boundary layer is added to an Ekman flow to obtain the advective velocity (u_A, v_A),

$$(u_A, v_A) = (u_E, v_E) + (u, v)_{z=1}. \qquad (2.8)$$

The Ekman flow v_E is taken to be meridional ($u_E = 0$) and of the form

$$v_E = (w_{E0}/2\pi\delta_E) \sin 2\pi y, \qquad (2.9)$$

so the Ekman pumping is

$$w_E = \delta_E v_{Ey} = w_{E0}\cos 2\pi y. \qquad (2.10)$$

The air–sea heat flux F_T is obtained from T_E and an imposed atmospheric surface temperature T_a by a linearized flux law,

$$F_T = -\gamma_s(T_E - T_a), \qquad (2.11)$$

where T_a is a linear function of y. The heat flux F_i through the base of the boundary layer is

$$F_i = -w(z = 1)T_1 + \gamma_0(\kappa_v/\delta_E)[T_E - T(z = 1)], \qquad (2.12)$$

and this serves as the upper boundary condition for the interior thermodynamic equation (2.5), which is solved in flux form. A temperature discontinuity is allowed at the base of the surface boundary layer so that in (2.12) $T_1 = T(z = 1)$ if $w(z = 1) > 0$ and $T_1 = T_E$ if $w(z = 1) < 0$. The nondimensional constant γ_0 controls the rate of diffusive heat transport from the surface layer into the interior.

The equations are solved essentially as in Samelson and Vallis (1997b), with no-flux and no-normal-flow conditions at the lateral and bottom boundaries. The frictional–geostrophic relations (2.1) and (2.2) may be inverted for the horizontal velocities, giving

$$u = -\gamma(\varepsilon p_x + f p_y), \quad v = \gamma(f p_x - \varepsilon p_y), \quad (2.13)$$

where $\gamma = (f^2 + \varepsilon^2)^{-1}$. A vertical integral of (2.4) over the entire domain, including the surface boundary layer where (2.13) are supplemented by the Ekman flow component according to (2.8), then yields a diagnostic equation (the depth-integrated vorticity equation)

$$\mathcal{H}(P) = w_E - W_0 \qquad (2.14)$$

for the depth-integrated (barotropic) pressure P, where

$$P = \int_0^1 p\, dz + \delta_E p(z = 1) \qquad (2.15)$$

and

$$\mathcal{H}(P) = \varepsilon\gamma\Delta_h P + (f^2 - \varepsilon^2)\gamma^2\beta P_x - 2\varepsilon f\gamma^2\beta P_y. \qquad (2.16)$$

In (2.14), w_E is the Ekman pumping velocity from (2.10), and $W_0 = w(z = 0) = 0$ at the flat bottom boundary. Thus, P depends only on the imposed mechanical forcing, w_E. Consistent with (2.8) and the assumption $\delta_E \ll 1$, the pressure p has been taken to be independent of z in the surface boundary layer so that the vertical integral of p over the fluid depth yields (2.15).

b. Nondimensionalization

Appropriate dimensional values for the variables and parameters described above may be obtained using the following scales for depth, length, Coriolis parameter, density, gravity, and vertical velocity, respectively: $D = 5 \times 10^3$ m, $L = 5 \times 10^6$ m, $f_* = f(35°N) = 8.4$ $\times 10^{-5}$ s^{-1}, $\rho_0 = 10^3$ kg m^{-3}, $g = 9.8$ m s^{-2}, and $W = 10^{-6}$ m s^{-1}.

From these, the following dimensional scales may be derived for horizontal velocity, time, density variations, temperature variations, buoyancy frequency, heat flux, and heat transport, respectively: $U = WL/D = 10^{-3}$ m s^{-1}, $t_* = D/W = L/U = 5 \times 10^9$ s $= 160$ yr, $\rho_* = (\rho_0 f_* UL)/(gD) = 8.6 \times 10^{-3}$ kg m$^{-3} \approx 0.01\sigma_\theta$, $T_* = \rho_*/(\rho_0\alpha_T) = 0.086$ K, $N_0 = (g\rho_*/(\rho_0 D))^{1/2} = 1.3 \times 10^{-4}$ s$^{-1} = 0.075$ cph, $H_f = \rho_0 c_p W T_* = 0.34$ W m^{-2}, and $H_F = H_f L^2 = 0.9 \times 10^{13}$ W, where the values $\alpha_T = 10^{-4}$ K^{-1} and $c_p = 4000$ J kg^{-1} K^{-1} have been used for the thermal expansibility and specific heat of seawater.

Dimensional scales for the vertical, horizontal, and biharmonic horizontal thermal diffusivities are then $K_v = WD = 5 \times 10^{-3}$ m^2 s^{-1}, $K_h = UL = 5 \times 10^3$ m^2 s^{-1}, and $\Lambda = UL^3 = 1.25 \times 10^{17}$ m^4 s^{-1}. The friction parameter ε and the air–sea flux coefficient γ_s are nondimensionalized by f_* and W, respectively. The nondimensional parameter $\gamma_0 = 2$ in all cases.

The value of the dimensional temperature scale, $T_* \approx 0.1$ K, is small compared to the scale of temperature variations in the ocean, and consequently the appropriate dimensionless temperature field in solutions of these equations have variations of order 100–200 units or more. The reason for the appearance of this small scale may be deduced from the balances assumed in the scaling. The scale is an estimate of the basinwide thermal contrast necessary to produce geostrophic horizontal motions that are comparable to those produced by surface Ekman pumping, assuming that 1) the Ekman-driven flow is distributed uniformly over the basin depth, 2) the horizontal scale of the Ekman divergence is the basin width, and 3) the horizontal and vertical scales for the thermal wind balance are the basin width and depth. In the ocean and in solutions of these equations (Samelson and Vallis 1997), the actual vertical scale for the penetration of the wind-driven flow, and thus also the characteristic vertical scale for the thermal wind balance, is small compared to the basin depth. The square of this small depth ratio estimates the ratio of T_* to observed basin-scale temperature differences.

In the discussion below, nondimensional values of the parameters will generally be quoted, with corresponding dimensional values given parenthetically. Thus, $\kappa_v = 0.01$ (0.5×10^{-4} m^2 s^{-1}) corresponds to nondimensional and dimensional vertical temperature diffusivities of 0.01 and $0.01 \times 5 \times 10^{-3}$ m^2 s$^{-1} = 0.5 \times 10^{-4}$ m^2 s^{-1}, respectively. For convenience, dimensional variables are used in the figures for temperature (reported on the Kelvin scale, but relative to an arbitrary constant), velocity, and related quantities.

The parameters $f_0 = 1, \beta = \beta_*(35°N)L/f_* = 1.1$, corresponding to a northern hemisphere basin with a central latitude of 35°N at $y = y_0 = 0.5$. The equations were discretized on $65 \times 65 \times 64$ or $65 \times 65 \times 32$ grids, stretched in the vertical to enhance resolution in

the upper thermocline. Steady-state solutions were obtained by time stepping to equilibrium.

c. Locally enhanced vertical diffusivity

To study the effect of locally enhanced vertical mixing, the vertical diffusivity is increased to a large value in a region adjacent to the eastern boundary so that κ_v depends on x according to

$$\kappa_v = G(x)\kappa_{v0}, \qquad (2.17)$$

where

$$G(x)$$

$$= \begin{cases} 1, & 0 < x < 0.9 \\ 1 + (G_0 - 1)(x - 0.9)/0.05, & 0.9 < x < 0.95 \\ G_0, & 0.95 < x < 1. \end{cases}$$

For the solution discussed below, $\kappa_{v0} = 0.004$ (0.2×10^{-4} m² s⁻¹) and $G_0 = 375$, so the vertical diffusivity is $\kappa_v = G_0 \kappa_{v0} = 1.5$ (75×10^{-4} m² s⁻¹) in a region of width 0.05 (250 km) adjacent to the eastern boundary and decreases linearly westward, reaching the uniform interior value κ_{v0} at $x = 0.9$, 0.1 units (500 km) west of the eastern boundary.

It should be emphasized here that the region of enhanced diffusivity in this calculation is not to be identified in a direct manner as a benthic boundary layer: its lateral extent is an order of magnitude too large, the dynamical equations are motivated even in the mixing region by large-scale asymptotics and not benthic boundary layer scaling, and vertical diffusivities of the present magnitude have been observed only in constricted overflows (e.g., Wesson and Gregg 1994); the Monterey Canyon observations of Lueck and Osborn (1985) yield a value that is five times smaller. Rather, the calculation is intended to serve as a simple and relatively accessible context, in which the interaction between localized regions of vertical mixing and a nearly adiabatic, planetary-geostrophic interior regime may be investigated. It is conceivable, however, that the amount of mixing that occurs in the present model eastern boundary layer might be consistent with reasonable boundary layer thicknesses and diffusivities if the mixing volume were distributed over the global benthic boundary layer. This is true particularly beneath 2500 m, where a substantial fraction of the ocean volume is within a few hundred meters of the bottom (e.g., Toole et al. 1997, Fig. 7).

3. Results

a. Spatially uniform vertical diffusivity

Before discussing the results obtained with the spatially variable vertical diffusivity, it is useful to review briefly the characteristics of two numerical solutions obtained with spatially uniform vertical diffusivity. The first has vertical diffusivity $\kappa_v = 0.004$ (0.2×10^{-4} m² s⁻¹), equal to the interior value of κ_v for the localized mixing case discussed below. The second has vertical diffusivity $\kappa_v = 0.116$ (5.8×10^{-4} m² s⁻¹), equal to the area-weighted average diffusivity for the localized mixing case. These solutions are qualitatively similar to many other previous solutions of large-scale circulation models based either on the planetary geostrophic equations or the primitive equations.

The forcing parameters for all solutions discussed here, including the localized mixing case, are the same as for the solutions described by Samelson and Vallis (1997b): $w_{E0} = 1$ (10^{-6} m s⁻¹), $T_a = 200(1 - y)$ (dimensional gradient ≈ 17 K/5000 km), and $\gamma_s = 5$ (0.4 m day⁻¹). The surface boundary layer thickness is $\delta_E = 0.005$ (25 m), the friction parameter $\varepsilon = 0.04$ (3.6×10^{-6} s⁻¹), and the horizontal diffusivity is $\kappa_h = 0.006$ (30 m² s⁻¹). The mechanical forcing (Ekman pumping) and the resulting depth-integrated pressure P are the same for all solutions discussed here. The P field is dominated by an anticyclonic subtropical gyre at the latitudes of Ekman downwelling ($0.25 < y < 0.75$), with a smaller cyclonic subpolar gyre to the north and a weak cyclonic tropical circulation to the south (Fig. 1).

For $\kappa_v = 0.004$, the surface temperature is close to the air temperature over most of the domain, with the exception of the western boundary current region, where northward advection maintains surface temperatures 3 K warmer than the local air temperature, and the extreme northern and southern portions of the domain, where surface temperatures fall 1–1.5 K short of the air temperature extremes (Fig. 1). The surface heat fluxes are correspondingly large in the western boundary current region and along the southern and northern boundaries (Fig. 2). The horizontal velocity field at the top of the interior, just beneath the surface boundary layer, is dominated by a baroclinic anticyclonic subtropical gyre (Fig. 1).

Midbasin cross sections of temperature versus depth for $\kappa_v = 0.004$ show the characteristic structure described by Samelson and Vallis (1997b): an adiabatic, ventilated thermocline regime on shallow isotherms that outcrop in the region of Ekman downwelling ($0.25 < y < 0.75$), with a weakly stratified layer of "subtropical mode water" at its base, and an advective–diffusive internal boundary layer regime separating the mode water from a nearly uniform abyss (Fig. 3). The temperature of the mode water layer (4 K $< T < 7$ K) increases westward across the basin (Fig. 3b); the abyssal temperature is roughly 1 K warmer than the coldest air temperature ($T_a = 0$, at $y = 1$). There is weak, roughly uniform upwelling from the abyss into the center of the internal boundary layer at subtropical latitudes, which drives a Stommel–Arons meridional abyssal flow (Fig. 4).

These thermocline regimes may be identified in vertical profiles of temperature T and buoyancy frequency
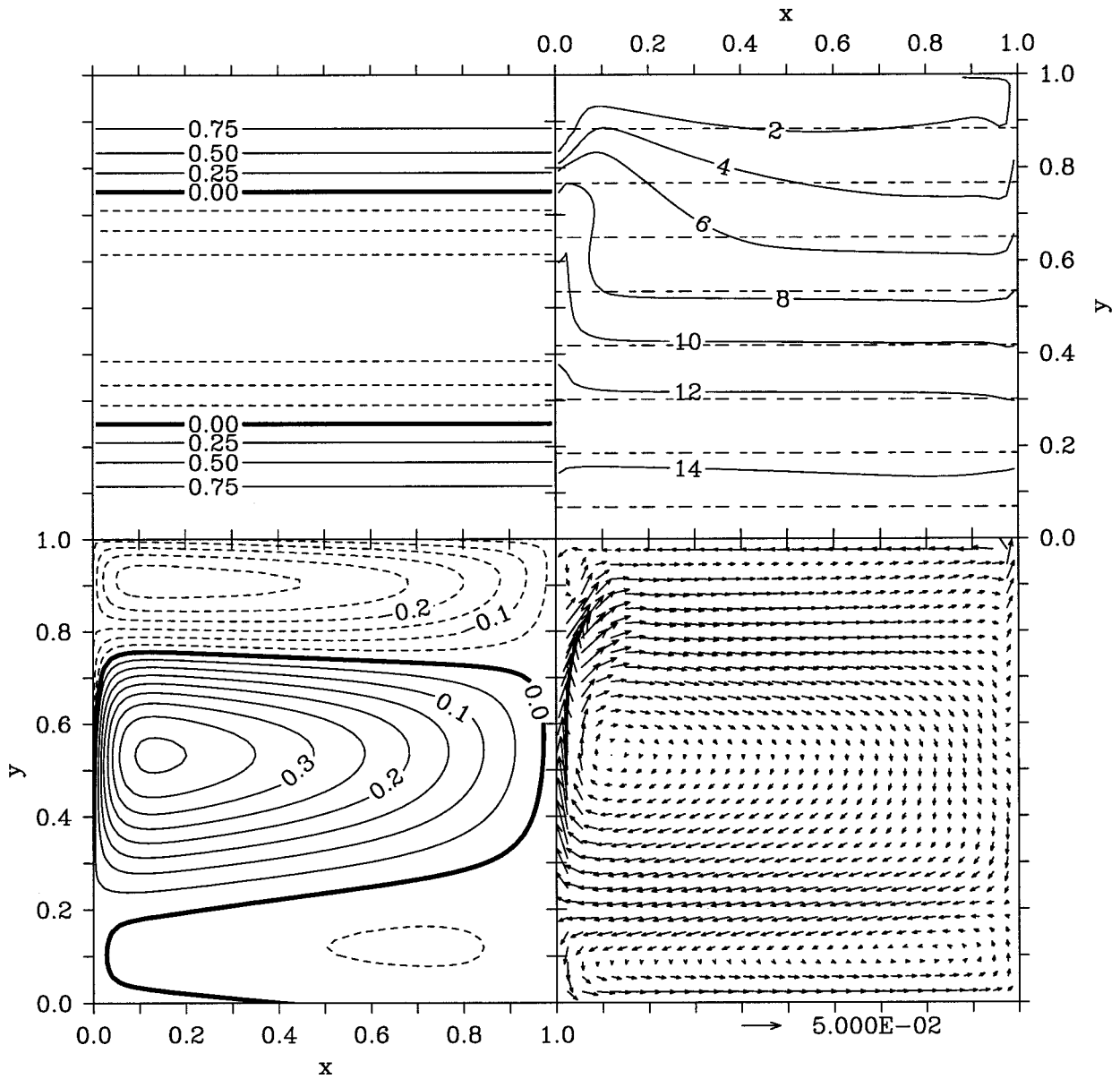
FIG. 1. Vertically integrated pressure P (lower left panel), Ekman pumping w_E (upper left), dimensional surface layer temperature T_E (K) (solid contours) and imposed air temperature T_a (dashed contours, contour interval 2 K) (upper right), and dimensional surface layer velocities (u_A, v_A) from (2.8) (m s^{-1}) (lower right) for the solution with $\kappa_v = 0.004$.

$N = T_z^{1/2}$ at the center of the basin for $\kappa_v = 0.004$ (Fig. 5). The surface maximum in N and the adjacent interior relative minimum below are the signatures of the adiabatic ventilated thermocline regime and the shallow subtropical thermostad (mode water). The interior maximum in N is the signature of the advective–diffusive internal boundary layer, which forms near the zero crossing of the vertical velocity (Samelson and Vallis 1997b). In the abyss, temperature is nearly uniform and N is small.

Although the present calculations are highly idealized, the basin-center N profile from the $\kappa_v = 0.004$

solution may be usefully compared with an observed buoyancy frequency profile from the central North Atlantic (Fig. 5). There is a rough correspondence between the model N and the observations for $z > 0.7$ (above 1500 m), but at greater depths the profiles differ qualitatively: the model stratification beneath the main thermocline is much too weak (N is much too small). Although the model is highly idealized, the rough agreement between model and observed stratification in the main thermocline for $\kappa_v = 0.004$ may be regarded as indirect theoretical support for a small (order 10^{-5} m^2 s^{-1}) interior turbulent diffusivity.
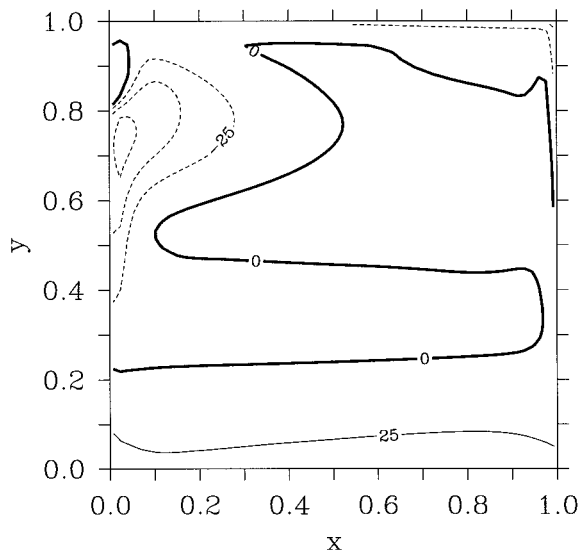
FIG. 2. Dimensional surface heat flux (W m^{-2}) for the solution with $\kappa_v = 0.004$.

FIG. 3. Meridional (a) and zonal (b) cross sections of dimensional temperature T (K) at $x = 0.5$ and $y = 0.5$, respectively, for the solution with $\kappa_v = 0.004$.

A more strongly stratified deep water column results if the magnitude of the vertical diffusivity is increased. In that case, the internal boundary layer thickens as the diffusivity increases, eventually extending all the way to the bottom. For $\kappa_v = 0.116$, the model deep stratification has roughly the strength of the observed deep stratification, particularly near middepth (Fig. 5). However, the upper thermocline structure for $\kappa_v = 0.116$ shows substantially less resemblance to the observations than for $\kappa_v = 0.004$, as the interior maximum in observed buoyancy frequency near $z = 0.85$ (750 m depth) has no counterpart for $\kappa_v = 0.116$. The solution with $\kappa_v = 0.116$ has a weak oscillatory time dependence, complicating the comparison, but the oscillation has only a small signal in the deep stratification. The oscillation is associated with modulations of a quasi-stationary dipolar pattern in surface heat flux that forms in the northeastern part of the subtropical gyre (Fig. 6).

In summary, solutions of the present planetary geostrophic model with uniform κ_v cannot simultaneously reproduce the observed qualitative structure of the stratification both in and beneath the main thermocline. The uniform vertical diffusivity gives rise, beneath the upper wind-driven fluid, to a single diffusive internal boundary layer characterized by a single vertical scale that is set by the value of the diffusivity κ_v. In contrast, the observed deep stratification is characterized by (at least) two vertical scales: one of a few hundred meters, at the base of the main thermocline (near 1000 m depth, or $z = 0.8$ nondimensionally), and a second, larger scale describing the roughly uniform stratification extending from the base of the main thermocline to near the bottom.

A similar discrepancy between observations and primitive equation models has been noted by Cummins
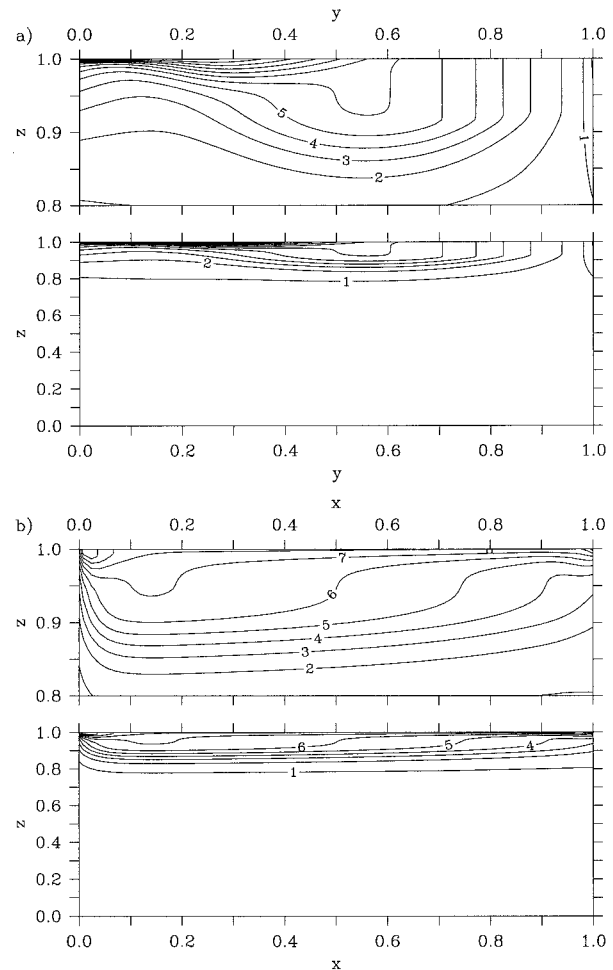
(1991), who demonstrated that a primitive equation model could reproduce an observed mean stratification profile if the vertical diffusivity was kept horizontally uniform but made to depend on depth, increasing rapidly beneath the main thermocline. The present study explores the alternative possibility that vertical mixing in the deep ocean is small over most of the ocean basin but large in localized regions.

b. Locally enhanced vertical mixing

In this section, the qualitative structure of a "localized mixing" solution, with a spatially variable vertical diffusivity, is described. The spatial dependence of the vertical diffusivity κ_v is given by (2.17) and (2.18): in a region adjacent to the eastern boundary, κ_v is enhanced by a factor of 375 over its interior value $\kappa_v = 0.004$. The particular value of the enhanced diffusivity was chosen, by trial and error, in order to give a deep stratification that is roughly comparable to observations. Solutions
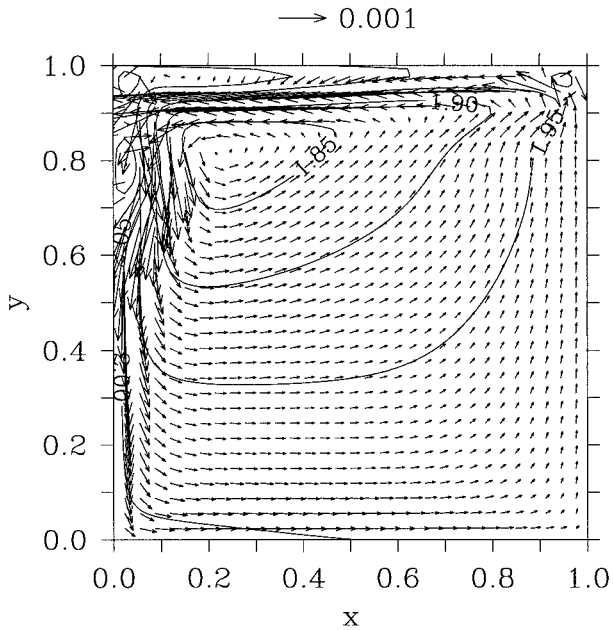
FIG. 4. Pressure contours and dimensional velocity vectors (m s^{-1}) at $z = 0.5$ for the solution with $\kappa_v = 0.004$.

FIG. 6. Dimensional surface heat flux (W m^{-2}) for the solution with $\kappa_v = 0.116$.

with different values of the enhanced diffusivity give qualitatively similar results. For the localized mixing solution, all model parameters except κ_v are the same as for the $\kappa_v = 0.004$ case described above. The imposed Ekman pumping and the resulting time-independent depth-integrated pressure P are as shown in Fig. 1.

The surface temperature is nearly equal to the imposed air temperature in the subtropical gyre interior (Fig. 7). Upwelling maintains surface temperatures below the local air temperature along the southern half of
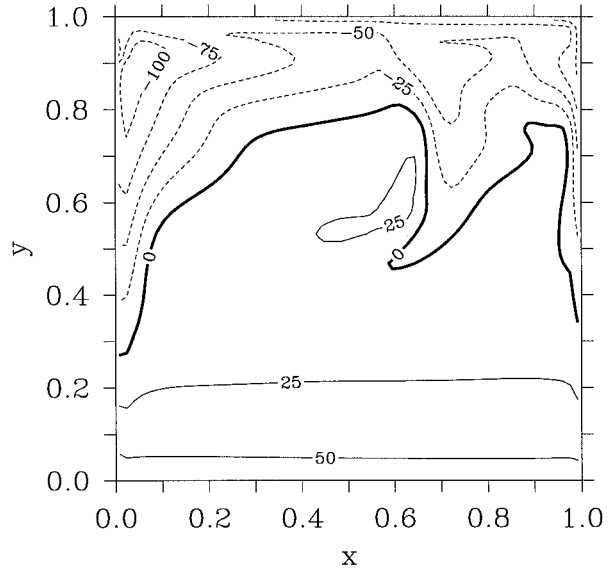
the eastern boundary and, by a lesser amount, along the southern boundary. Horizontal advection maintains surface temperatures above the local air temperature along the western and northern boundaries. The largest departures of surface temperature from local air temperature are roughly 9 K in the southeastern corner of the domain and 5 K in the northern part of the western boundary current. Relative to the $\kappa_v = 0.004$ solution, surface heating is enhanced along the eastern boundary, while cooling is enhanced along the western and northern boundaries and along the western boundary current extension in the interior (Fig. 8).
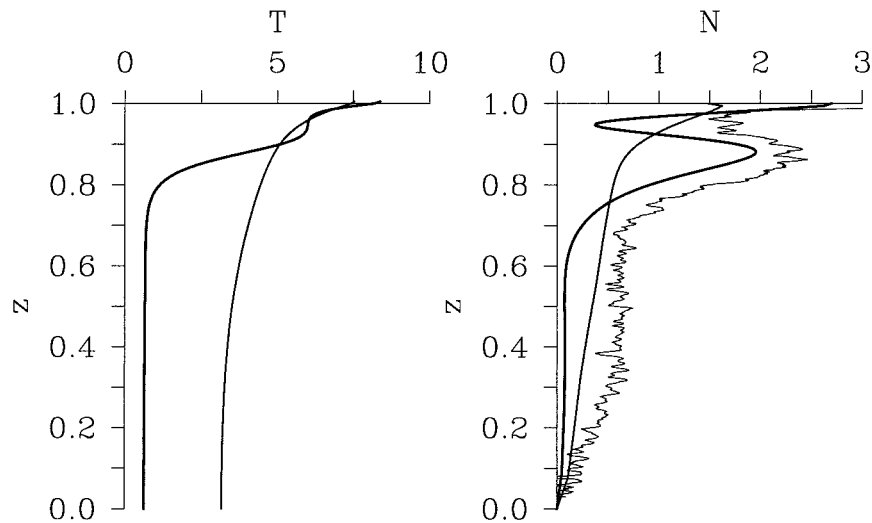

FIG. 5. Vertical profiles of dimensional temperature T (K) (left panel) and buoyancy frequency $N = T_z^{1/2}$ (cph) (right panel) at basin center, $(x, y) = (0.5, 0.5)$, for the solutions with $\kappa_v = 0.004$ (thick line) and $\kappa_v = 0.116$ (intermediate line). A profile of buoyancy frequency from 36°N, 45°W in the North Atlantic is also shown (right panel, thin line).
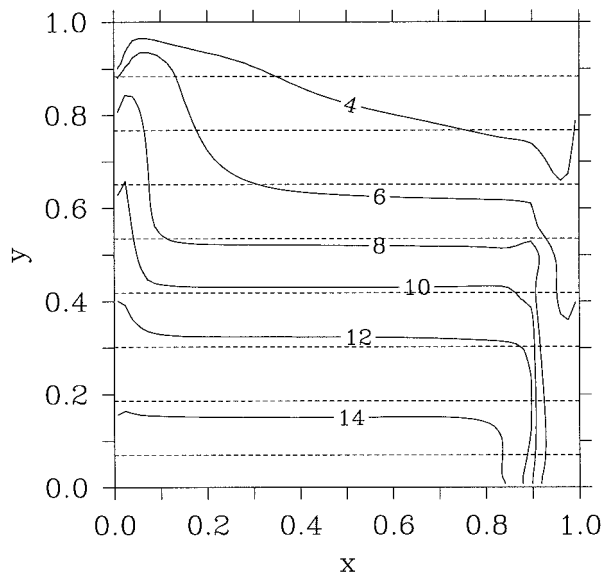
FIG. 7. Dimensional surface layer temperature T_E (K) (solid contours) and imposed air temperature T_a (dashed contours, contour interval 2 K) for the localized mixing solution.
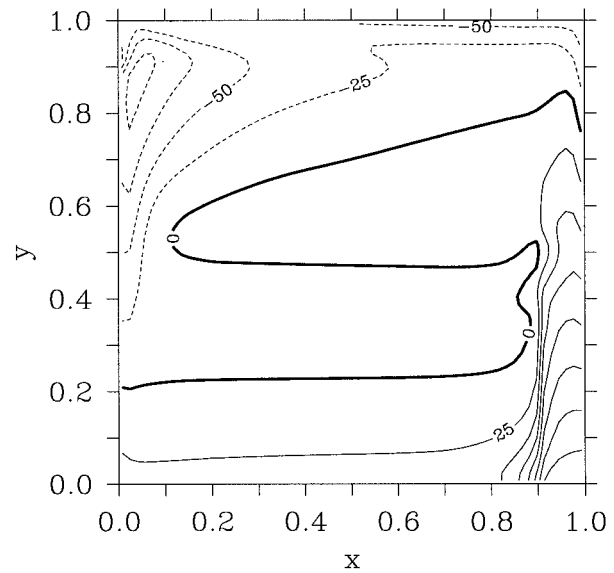

FIG. 8. Dimensional surface heat flux (W m^{-2}) for the localized mixing solution.

The vertical profile of buoyancy frequency $N = T_z^{1/2}$ at basin center shows a deep diffusive thermocline with two distinct vertical scales: an internal boundary layer centered at the base of the ventilated thermocline near $z = 0.8$ (1000-m depth) and an abyssal thermocline beneath, with vertical scale comparable to the total depth of the fluid (Fig. 9). The stratification beneath the internal boundary layer, in the depth range $0 < z < 0.7$), is comparable to the uniform diffusivity case with $\kappa_v = 0.116$ (Fig. 9).

Temperature cross sections at midbasin have a structure above the internal boundary layer that is similar to the uniform diffusivity case with $\kappa_v = 0.004$ (Figs. 10 and 3): strong near-surface stratification on ventilated isopycnals overlying a weakly stratified layer at the base of the ventilated thermocline. The mixed layer at the subtropical–subpolar gyre boundary is deeper in the localized mixing case than in the $\kappa_v = 0.004$ case (Figs. 3a and 10a), in order to support the enhanced northward flow of warm water across the gyre boundary (Figs. 1 and 11a; see also Figs. 13 and 16 below). Since this depth effectively sets the eastern boundary condition for the base of the moving fluid in the ventilated thermocline, the result is a thicker mode water layer and a deeper thermocline throughout the subtropical gyre: the maximum in T_z at basin center is 0.05 units (250 m) deeper for the localized mixing solution than for $\kappa_v = 0.004$ (Fig. 9). The increased diffusivity enhances the northward flow of warm water by drawing abyssal fluid up through the internal thermocline into the subtropical mode water layer (4 K $< T <$ 7 K), from where it must return northward to the subpolar gyre to cool and sink.

The near-surface circulation is dominated by westward zonal flow in the southern half of the interior,

northward flow along the western boundary, and eastward flow in the northern half of the interior (Fig. 11a). The pattern of flow in the abyssal interior is essentially the reverse of the near-surface pattern (Fig. 11b). The circulation is closed by upwelling along the southern half of the eastern boundary and downwelling along the northern boundary (Fig. 12). The abyssal vertical velocity for $\kappa_v = 0.004$ is similar to that shown in Fig. 10 of Samelson and Vallis (1997), with weak and nearly uniform upwelling over most of the basin and downwelling confined to the northern boundary and the northern part of the western boundary. For $\kappa_v = 0.116$, the abyssal vertical velocities are an order of magnitude larger than for $\kappa_v = 0.004$ but have a similar spatial distribution, except in the northeastern part of the subtropical gyre where there are large variations associated with a quasi-stationary dipolar feature (cf. Fig. 6 and discussion above).

The large-scale flow pattern thus combines zonal motion in the interior and along the northern boundary with meridional motion along the western boundary. The upwelling fluid that leaves the diffusive eastern boundary layer enters the essentially adiabatic interior and flows westward to the western boundary, then northward to the subpolar gyre, where it cools and sinks. It returns southward in a deep western boundary current and crosses the interior zonally to the east, arriving at the eastern boundary at depth. In the southern half of the eastern boundary layer ($0 < y < 0.5$), the deeper fluid moves northward and the shallower fluid moves southward. This boundary layer flow pattern is consistent with the Sverdrup vorticity balance and the existence of a middepth upwelling maximum in the southern part of the boundary layer, resulting in vortex stretching at depth and vortex compression above. In the northern
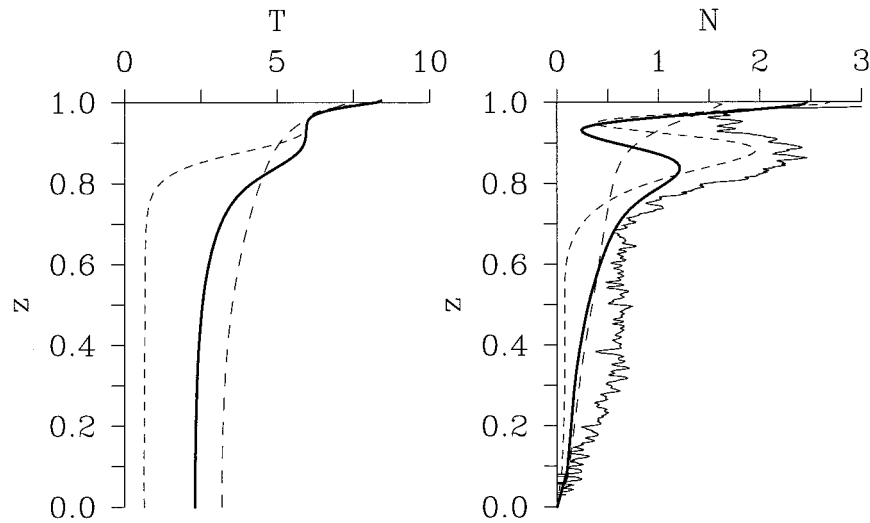
FIG. 9. Vertical profiles of dimensional temperature T (K) (left panel) and buoyancy frequency $N = T_z^{1/2}$ (cph) (right panel) at basin center, $(x, y) = (0.5, 0.5)$, for the localized mixing solution (thick line). The corresponding profiles for the $\kappa_v = 0.004$ (short dashes) and $\kappa_v = 0.116$ (long dashes) solutions are also shown, along with a profile of buoyancy frequency from 36°N, 45°W in the North Atlantic (right panel, thin line).

half of the boundary layer, cooling and sinking prevail, and the flow is generally in the opposite sense as in the southern half. Associated with the zonal interior flow in the southern subtropical gyre is a nearly uniform north–south slope of interior isotherms that extends to the southern domain boundary (Fig. 10a).

In summary, the localized mixing gives rise to a deep thermocline with two distinct vertical scales, one associated with the internal boundary layer and a second that is set in the mixing region. The interior abyssal thermocline is controlled by zonal flows that originate in the western and eastern boundary layers (Fig. 11). The deep stratification is similar in the boundary layer and in the adjacent interior, but the shallow stratification contrasts dramatically as the warm fluid of the ventilated thermocline accumulates near the surface outside the cool eastern boundary layer. The internal boundary layer forms in the interior between the ventilated and abyssal thermocline regimes.

c. Meridional overturning and heat transport

The strength of the zonally averaged meridional overturning circulation is similar in the localized mixing case and the case with uniform vertical diffusivity $\kappa_v = 0.116$, for which κ_v is equal to the area-averaged κ_v from the localized mixing case (Figs. 13a,c). For $\kappa_v = 0.004$, the deep overturning circulation is an order of magnitude weaker (Fig. 13b).

The zonally integrated meridional heat transport is larger by half for $\kappa_v = 0.116$ than it is for the localized mixing case, despite the closer similarity in the strength of the meridional overturning circulations (Fig. 14). In contrast, for $\kappa_v = 0.004$ the heat transport is smaller by

only about half (Fig. 14), while the overturning is an order of magnitude weaker (Fig. 13). This behavior may be understood by examining the volume distribution and western boundary current transport in temperature classes and the distribution of net diffusive fluxes through isothermal surfaces.

For $T > 7$ K, the volume distribution by temperature class for the localized mixing solution resembles that for $\kappa_v = 0.004$, while for $T < 7$ K, it is similar to that for $\kappa_v = 0.116$ (Fig. 15). Thus, a transition occurs near the warmest temperature that develops in the eastern boundary mixing region in the localized mixing case. Above, in warmer water, the localized mixing has little effect, and the volume distributions for the localized mixing solution and the $\kappa_v = 0.004$ solution are similar. Below, in colder water, the volume distributions for localized mixing and for $\kappa_v = 0.116$ are similar (Fig. 15). This is consistent with the comparison of vertical profiles of buoyancy frequency in the previous section (Fig. 9). The mode water temperature classes $4 \text{ K} < T < 7$ K have increased volume in the localized mixing case, so the effect of the localized mixing is not confined beneath the internal thermocline. The dimensionless integrated heat content is 13 for $\kappa_v = 0.004$, 34 for the localized mixing case, and 46 for $\kappa_v = 0.116$.

For $T < 7$ K, the expression of the meridional overturning cell in the western boundary current transport distribution is similar for $\kappa_v = 0.116$ and for the localized mixing case, but much weaker for $\kappa_v = 0.004$ (Fig. 16). The meridional heat transport for $\kappa_v = 0.004$ arises primarily from northward western boundary current transport of warm water from the upper thermocline, with only a small contribution from the deeper, diffusively driven overturning. The larger heat transport
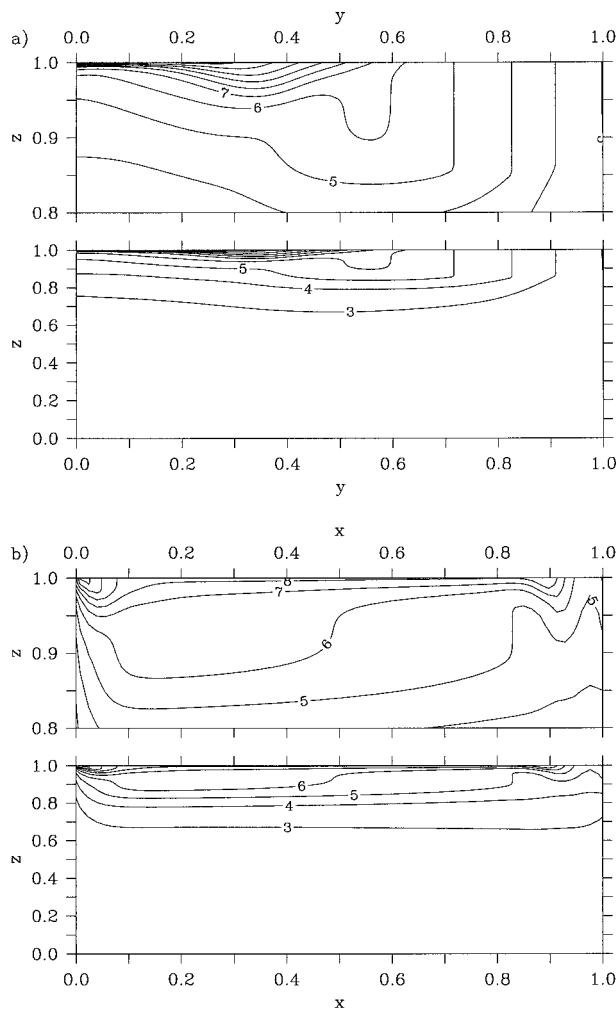
a)

b)

FIG. 10. Meridional (a) and zonal (b) cross sections of dimensional temperature T (K) at $x = 0.5$ and $y = 0.5$, respectively, for the localized mixing solution.

for the localized mixing case, relative to $\kappa_v = 0.004$, is associated with the stronger overturning cell with enhanced northward transport in the mode water temperature classes (4 K $< T <$ 7 K) and enhanced southward transport of abyssal ($T <$ 3 K) fluid. The southward transport of cold fluid occurs almost entirely in the temperature range 2.15 K $< T <$ 2.3 K, a narrower range than suggested by Fig. 16. The transport of warm water ($T >$ 7 K) is comparable for the localized mixing case and for $\kappa_v = 0.004$ (Fig. 16). The larger heat transport for $\kappa_v = 0.116$, relative to the localized mixing case, is associated with larger western boundary current transport of fluid in the temperature classes warmer than the mode water, $T >$ 7 K, that is, in those classes that have additional volume for $\kappa_v = 0.116$. Thus, for $\kappa_v = 0.116$, the additional heat transport relative to the localized mixing case arises from enhanced diffusive production of warm water in the upper ventilated thermocline.

The distributions of diffusive heat flux across iso-

thermal surfaces (Fig. 17) provide an alternate view of this structure. The $\kappa_v = 0.116$ solution has much larger fluxes across the isothermal surfaces with $T >$ 8 K than the localized mixing solution, while the fluxes for $T <$ 6 K are comparable. Conversely, the fluxes for the localized mixing and $\kappa_v = 0.004$ solutions are similar for $T >$ 8 K but differ for $T <$ 7 K. These distributions show explicitly that the spatially localized mixing is also localized with respect to temperature class, as it does not affect fluid that is warmer than the warmest surface fluid in the mixing region. They also demonstrate that the net diffusive fluxes across isothermal surfaces are controlled in the present calculations by vertical diffusion, not horizontal diffusion across the steeply sloping isotherms of the western boundary current.

With localized mixing, it can be anticipated that the temperature of the surface fluid in the eastern upwelling region will depend on the relaxation coefficient γ_s for air–sea heat exchange. Consequently, additional warm water ($T >$ 7 K) could be produced in that case if γ_s were increased sufficiently in that region. This would modify the heat transport and warm water transport distributions by temperature class.

4. Discussion

a. Scaling

The principal qualitative difference in thermocline structure between the solutions with and without locally enhanced vertical diffusion is the existence of a deep stratification with two distinct vertical scales. Since the absence of this structure in the deep stratification was an important discrepancy between observations and previous model results obtained with uniformly small vertical diffusivity (Samelson and Vallis 1997b), this difference is of interest. In this section, the manner in which the locally enhanced vertical diffusion controls the stratification beneath the internal thermocline is briefly examined.

A variant of the traditional advective–diffusive thermocline scaling (Welander 1971; Pedlosky 1987) may be used to describe the flow in the eastern boundary layer. The dimensional thermal wind, continuity, and thermodynamic equations may be estimated as

$$fU_b/D \sim g\alpha\Delta T/L \tag{4.1}$$

$$fV_b/D \sim g\alpha\Delta T/(\delta_b L) \tag{4.2}$$

$$U_b/(\delta_b L) \sim V_b/L \sim W_b/D \tag{4.3}$$

$$W_b \sim \kappa_b/D. \tag{4.4}$$

Here the subscripts b on the velocity scales U_b, V_b, W_b, and the diffusivity κ_b indicate values in the eastern boundary layer. The aspect ratio δ_b is the ratio of the boundary layer width to the basin width. The numerical solutions suggest that the depth scale D for the abyssal thermocline is the same in the boundary layer and the
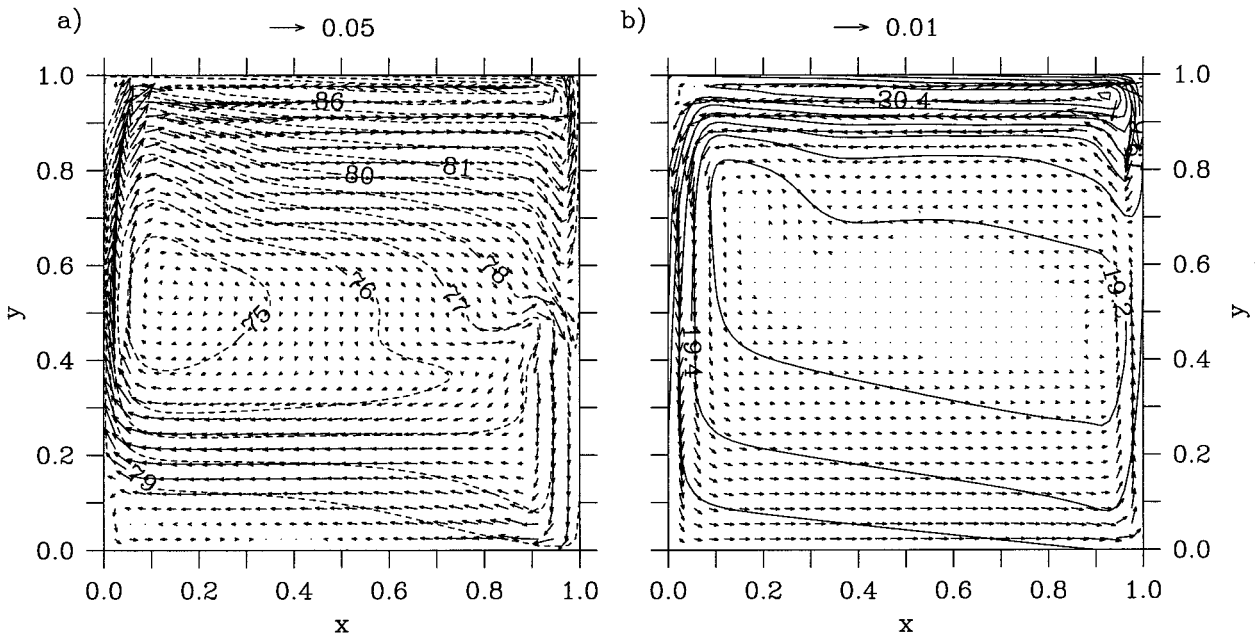
FIG. 11. Pressure contours and dimensional velocity vectors (u, v) (m s^{-1}) at (a) $z = 1$ and (b) $z = 0.4$ for the localized mixing solution. The velocities shown in (a) are the uppermost interior velocities and do not include an Ekman component.

interior, so D has no subscript. The three-dimensional balance in the continuity equation is appropriate for a boundary layer that exchanges fluid with the interior at first order.

The scale ΔT measures the temperature variations between the boundary layer and the interior and between the surface and the bottom in the boundary layer. In the numerical solutions, these differences are both approximately half the north–south air temperature difference.

FIG. 12. Dimensional vertical velocity (10^{-4} m s^{-1}) at $z = 0.64$ for the localized mixing solution.

A scaling estimate of ΔT may be obtained by balancing the air–sea flux with the downward diffusive heat flux in the boundary layer,

$$\kappa_b \Delta T/D \sim \gamma_s(\Delta T_s - \Delta T), \qquad (4.5)$$

which yields

$$\Delta T \sim \frac{\gamma_s}{\kappa_b/D + \gamma_s}\Delta T_s. \qquad (4.6)$$

For simplicity, assume that γ_s is varied with κ_b such that $\gamma_s \sim \kappa_b/D$. Then $\Delta T \sim \Delta T_s$, and the temperature scale ΔT may be consistently estimated as a fixed fraction of the north–south air temperature difference.

The unknown velocities may be eliminated from (4.1)–(4.4) in favor of D, which gives

$$D \sim (\delta_b \kappa_b fL^2/(g\alpha\Delta T))^{1/3}. \qquad (4.7)$$

By the above argument, the temperature scale ΔT may be taken as a fixed fraction of ΔT_s if γ_s is varied proportionately to $\kappa_b/D \sim \kappa_b^{2/3}$. The estimate (4.7) for D is then equivalent to the advective–diffusive thermocline depth scale, with an effective diffusivity $\kappa_A = \delta_b \kappa_b$ appearing in place of the usual uniform interior diffusivity. This effective diffusivity may be interpreted as an area-weighted diffusivity, if the small contribution from the small interior diffusivity is neglected. The notion of an area-weighted effective diffusivity is familiar from tracer budget analysis; the present scaling suggests that it may be relevant also to the large-scale dynamics. The similarity noted above of the deep stratification for the localized mixing and $\kappa_v = 0.116$ (where $\kappa_v = 0.116$ is the area-weighted average of the localized mixing κ_v)
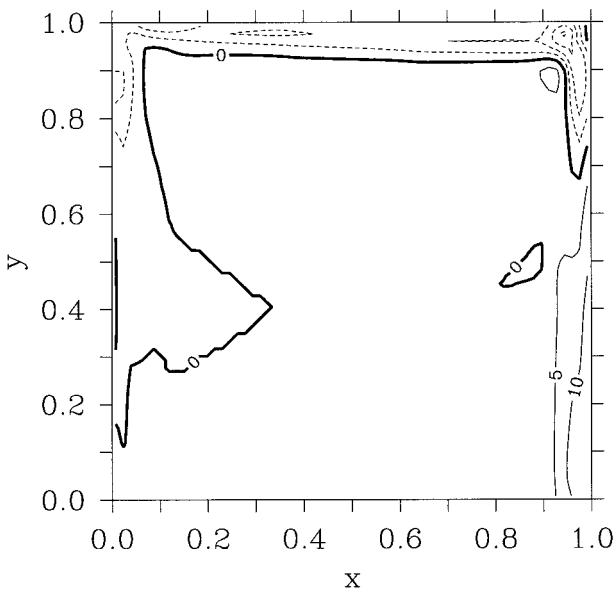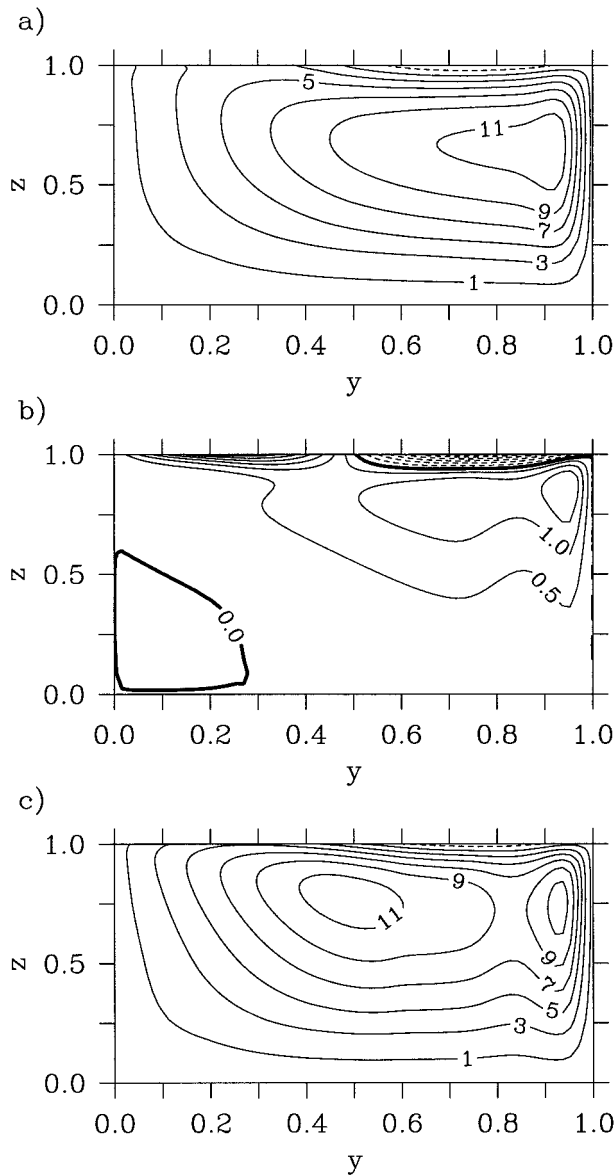
a)

b)

c)

FIG. 13. Dimensional meridional overturning streamfunctions (10^6 m^3 s^{-1}) for zonally averaged flow for the (a) localized mixing, (b) $\kappa_v = 0.004$, and (c) $\kappa_v = 0.116$ solutions. The sense of the circulation is clockwise around maxima.

solutions (Fig. 9) supports this conclusion. For $f = 10^{-4}$ s^{-1}, $L = 5 \times 10^8$ cm, $g = 980$ cm s^{-2}, $\alpha = 10^{-4}$ K^{-1}, $\Delta T = 10$ K, and a small uniform interior diffusivity $\kappa_{v0} = 0.2 \times 10^{-4}$ m^2 s^{-1}, the advective–diffusive scale gives a thermocline depth scale of 170 m. With $\delta_b = 0.1$ and $\kappa_b = 375\kappa_{v0}$, this scale increases by the factor $(\delta_b\kappa_b/\kappa_{v0})^{1/3} \approx 3.3$ to 570 m. The effective increase in the vertical scale of the abyssal interior stratification due to the locally enhanced mixing is roughly twice this factor, since the relevant vertical scale controlling the abyssal stratification in the small diffusion limit is not the advective–diffusive scale but the internal boundary layer
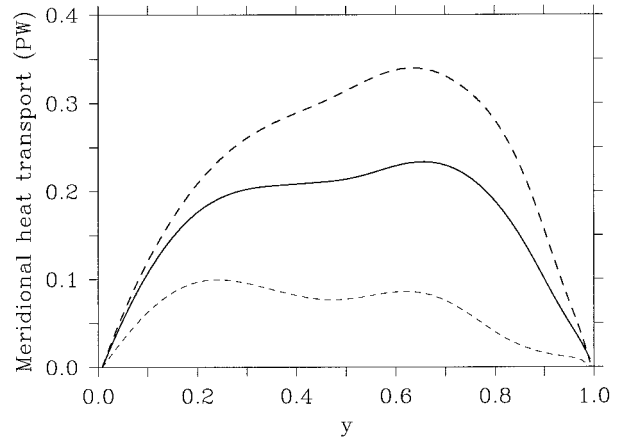
scale (Samelson and Vallis 1997b), which for these parameter values is roughly half as large ($\approx$100 m) as the advective–diffusive scale. An increase in vertical scale of the abyssal stratification of this magnitude is generally consistent with the numerical results. However, the scaling (4.7) has not been verified in detail, in part because the small variations with depth of the abyssal stratification, and the difficulty of separating the upper abyss from the lower internal thermocline, make reliable estimates of an abyssal thermocline vertical scale difficult to obtain. The abyssal depth scale of the midbasin profile of T_z (for which the square root $N = T_z^{1/2}$ is shown in Fig. 9) appears to be within a factor of 2 of the 570-m estimate, as T_z decreases from 30 to 10 (roughly a factor of e^{-1}) from $z = 0.6$ to $z = 0.4$ (1000 m).

The establishment of the advective–diffusive heat balance in the mixing region is implicit in this scaling. In the numerical solution, however, the associated upwelling must be generated by horizontal pressure gra-

FIG. 14. Dimensional zonally integrated northward heat transport (PW) vs latitude y for the solutions with localized mixing (solid line), $\kappa_v = 0.116$ (thick long dashes), and $\kappa_v = 0.004$ (thin short dashes).
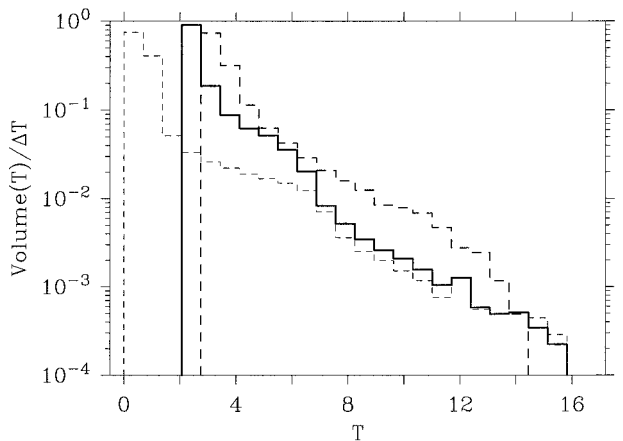

FIG. 15. Volume distribution by dimensional temperature class (K) for the solutions with localized mixing (thick solid line), $\kappa_v = 0.116$ (thick long dashes), and $\kappa_v = 0.004$ (thin short dashes).
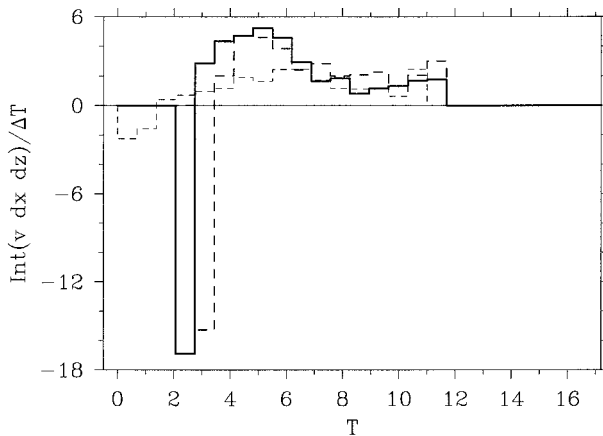
FIG. 16. Dimensional western boundary current transport (10^6 m^3 s^{-1}) by temperature class (K) $\int_{T_-}^{T_+} v \, dx \, dz/\Delta T$, $T_\pm = T \pm \Delta T/2$, $\Delta T = 8T_*$) for the solutions with localized mixing (thick solid line), $\kappa_v = 0.116$ (thick long dashes), and $\kappa_v = 0.004$ (thin short dashes). The eastern limit of the western boundary current was taken to be $x = 0.1$.

dients that drive horizontally convergent motion in the eastern boundary layer. This convergence is primarily planetary geostrophic ($u_x + v_y \approx -\beta v/f \approx -w_z$); friction is smaller, though not negligible. Its generation may be understood as follows. At depth, downward diffusion of heat warms deep fluid adjacent to the eastern boundary, generating a zonal temperature gradient and meridional geostrophic shear in the boundary layer. This shear supports northward boundary layer flow that increases from the bottom, causing a divergence at the southern boundary that is balanced by zonal inflow. Near the surface, the downward heat diffusion cools the boundary layer fluid relative to the interior, generating a zonal temperature gradient of opposite sign that supports southward geostrophic flow in the boundary layer, whose convergence at the southern boundary is balanced by zonal outflow. The local mass balance would require downwelling to balance the deep divergence and shallow convergence adjacent to the southern boundary if horizontal inflow and outflow were prevented; this downwelling, which would be inconsistent with a local advective–diffusive balance, does not occur. The northward extent of the region of downward heat diffusion is limited by the northward decrease of the air temperature, and the corresponding meridional flow convergence and divergence that result from this confinement are balanced by upwelling in the boundary layer, which allows the establishment of the advective–diffusive heat balance in the mixing region.

Although the basin width L nominally enters the scaling (4.7), the physical argument suggests that the abyssal stratification is controlled by an advective–diffusive balance that is confined entirely to the mixing region. Consequently, the abyssal stratification should be approximately independent of the area of the adiabatic interior. This conjecture is supported by the results of an additional numerical experiment in which a localized
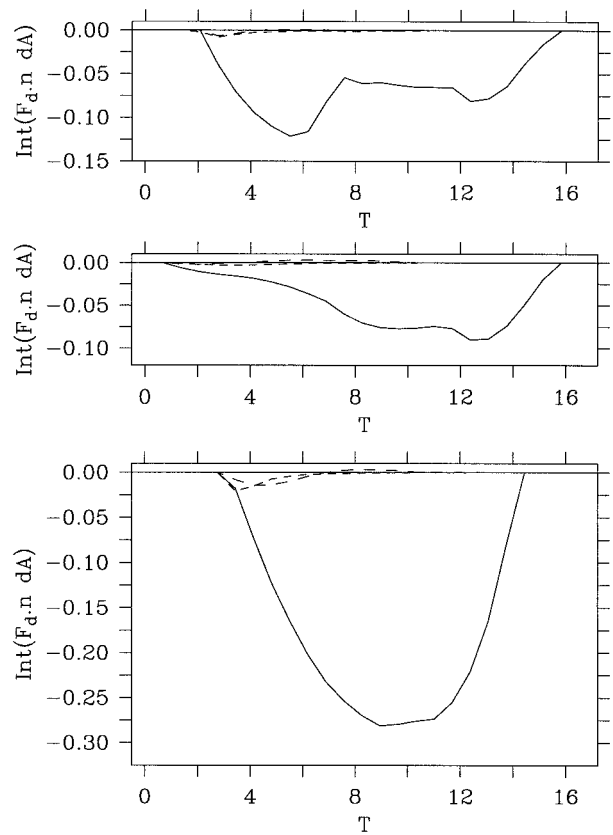

FIG. 17. Dimension integrated interior diapycnal diffusive fluxes (PW) from vertical (solid line), zonal (long dashes), and meridional (short dashes) diffusion for the solutions with (a) localized mixing, (b) $\kappa_v = 0.004$, and (c) $\kappa_v = 0.116$.

mixing solution was computed in a basin with doubled zonal extent but equal mixing region width. The abyssal stratification was not strongly affected by the increase in basin width. This suggests that the vertical scale of the deep, diffusive thermocline in the present model may be controlled by the area-integrated, not area-averaged, effective vertical diffusivity.

b. Other experiments

The numerical experiments presented here were selected from a number of such experiments carried out over the last two years with various versions of the planetary geostrophic model. Others included enhanced diffusivity at other boundaries or in localized interior regions. Details of the resulting solutions depend strongly on the distribution of the enhanced mixing regions. For example, enhanced mixing along the western boundary leads to weaker zonal abyssal flow and a complex interaction between the diffusively driven circulation and the western boundary current. Other variations have not yet been explored, for example, dependence on γ_s and δ_E. In general, however, the development of a deep thermocline with two distinct vertical

scales appears to be robust when vertical mixing is strongly localized and extends to the surface in the warm region. This is the main result reported here; a more complete exploration of the properties of these solutions is left to future work.

Related numerical experiments with a primitive equation ocean model in a similar geometry have recently been carried out by Marotzke (1997). No wind forcing was applied, and both temperature and salinity effects were included, so the results cannot be compared directly. Solutions were obtained on a $17 \times 17 \times 15$ grid. The horizontal diffusivity was 10^3 m^2 s^{-1} (corresponding to dimensionless $\kappa_h = 0.2$, 33 times greater than the value used here), sufficiently large that diffusion across the tilted isopycnals of the western boundary current was an important component of the interior flux balance. The vertical diffusivity was set to zero at all grid points except those adjacent to a lateral boundary, where it was varied between zero and 100×10^{-4} m^2 s^{-1}. As in the present solutions, vertical motion was confined primarily to the regions of large vertical diffusivity with upwelling along both eastern and western boundaries and downwelling largest in the northeastern corner, and meridional motion was weak in the interior. Meridional overturning was proportional to $\kappa_v^{2/3}$, consistent with a scaling argument similar to that given above. In contrast to the present results, a solution with uniform vertical diffusivity had a smaller meridional heat transport than the boundary mixing solution with equal area-weighted vertical diffusivity. Solutions with boundary κ_v greater than 30×10^{-4} m^2 s^{-1} were time dependent. The effect of the localized mixing on the qualitative structure of the deep stratification was not discussed.

5. Summary

The numerical experiments summarized here demonstrate that localized regions of intensified vertical mixing can exert strong control over the deep stratification and circulation of a planetary geostrophic ocean model when the localized mixing extends to the surface in the warm region. The subtropical gyre ventilated and internal thermoclines that arise in the model for uniform small interior diffusivity persist in the present solutions, but the abyssal structure changes markedly. Zonal flows driven by planetary-scale divergence in the mixing region carry deep, diffusively warmed fluid into the nearly adiabatic interior beneath the main thermocline and overwhelm the weak Stommel–Arons meridional abyssal flow driven by interior diffusion through the main thermocline. In contrast to results obtained with a uniform vertical diffusivity, the deep stratification has two distinct vertical scales, one associated with the internal boundary layer at the base of the ventilated thermocline and a second set by an advective–diffusive balance in the mixing region. This deep thermocline structure is reminiscent of observed deep ocean stratification.

In these solutions with simply connected, single-hemisphere basin geometry, the generation of deep stratification with comparable buoyancy frequency to observed values requires a large diffusivity ($\approx$100 cm^2 s^{-1}) over a broad area (boundary layer $\approx$500 km wide). However, the depth scale of the deep diffusive thermocline appears to depend on the area-integrated, rather than area-averaged, vertical diffusivity, so it is conceivable that the amount of mixing that occurs in the present model eastern boundary layer might be consistent both with the observed deep thermocline structure and with reasonable boundary layer thicknesses and diffusivities, if the mixing volume were distributed over the global benthic boundary layer.

The circulation that develops in the model effectively contains a single source of deep water. Although the deep western boundary current extends upward from the bottom to the base of the main thermocline ($z \approx 0.8$) at the subpolar–subtropical gyre boundary, the fluid that it carries has a nearly uniform temperature that is colder than any of the fluid above middepth ($z \approx 0.5$) in the central subtropical gyre. The middepth subtropical thermocline is filled with warmer deep water that has entered the subtropical gyre as cold deep water in the deep western boundary current and has then been modified in the eastern boundary mixing region. It is not filled with a warmer brand of deep water that might in principle have flowed southward from the subpolar gyre (where fluid of corresponding temperature does exist) and directly into the interior from an upper limb of the deep western boundary current.

By contrast, it is well known that the deep water masses in the North Atlantic have several distinct sources, which originate in the polar and marginal seas. Sources for North Atlantic Deep Water, for example, include water from the Labrador Sea and from polar sea overflows, and together span the density range over which North Atlantic Deep Water is observed in the abyssal interior. One might wish immediately to attribute the observed abyssal stratification to the difference in densities between these separate source waters. However, the relative formation rates of these source waters do not by themselves determine the relative volume distribution of the corresponding water masses in the deep ocean. If, for example, there were no mixing at all in the deep ocean, the densest brand of deep water would inevitably fill the entire deep basin, while less dense source waters would never reach the abyss. Thus, if the large-scale circulation and property distributions in the deep ocean are assumed to be approximately in steady state (possibly a poor assumption, but one that appears consistent with available observations), then it follows that mixing must influence the deep circulation and stratification. Consequently, it is not appropriate to attribute the observed abyssal stratification solely to the existence of differentiated source waters.

Nonetheless, it should be emphasized that the density distribution of deep water sources is much broader in

the North Atlantic than in the present model. The fluid that enters the subtropical North Atlantic beneath the main thermocline is not confined, as here, to a narrow range of the coldest temperature classes that are found at subtropical latitudes. Thus, while the present calculations illustrate that locally intensified mixing far from the deep water source can support the differentiation of abyssal waters and the consequent development of deep stratification, they also suggest that such mixing is not itself sufficient to induce the observed differentiation of abyssal source waters, as the circulation continues to prefer instead to replenish itself from the densest source alone.

REFERENCES

Armi, L., 1978: Some evidence for boundary mixing in the deep ocean. *J. Geophys. Res.,* **83,** 1971–1979.

Colin de Verdiere, A., 1988: Buoyancy driven planetary flows. *J. Mar. Res.,* **46,** 215–265.

——, 1989: On the interaction of wind and buoyancy driven gyres. *J. Mar. Res.,* **47,** 495–633.

Cummins, P., 1991: The deep water stratification of ocean general circulation models. *Atmos.–Ocean,* **19,** 563–575.

de Szoeke, R., 1995: A model of wind- and buoyancy-driven ocean circulation. *J. Phys. Oceanogr.,* **25,** 918–941.

Gregg, M., 1987: Diapycnal mixing in the thermocline: A review. *J. Geophys. Res.,* **92,** 5249–5286.

Hogg, N., 1987: A least-squares fit of the advective–diffusive equations to Levitus Atlas data. *J. Mar. Res.,* **45,** 347–375.

Ledwell, J., A. Watson, and C. Law, 1993: Evidence for slow mixing across the pycnocline from an open-ocean tracer-release experiment. *Nature,* **364,** 701–703.

Lueck, R., and T. Osborn, 1985: Turbulence measurements in a submarine canyon. *Contin. Shelf Res.,* **4,** 681–698.

Luyten, J., J. Pedlosky, and H. Stommel, 1983: The ventilated thermocline. *J. Phys. Oceanogr.,* **13,** 292–309.

Marotzke, J., 1997: Boundary mixing and the dynamics of three-dimensional thermohaline circulations. *J. Phys. Oceanogr.,* **27,** 1713–1728.

Munk, W., 1966: Abyssal recipes. *Deep-Sea Res.,* **13,** 707–730.

Pedlosky, J., 1987: *Geophysical Fluid Dynamics.* 2d ed. Springer-Verlag, 710 pp.

Polzin, K., J. Toole, J. Ledwell, and R. Schmitt, 1997: Spatial variability of turbulent mixing in the abyssal ocean. *Science,* **276,** 93–96.

Salmon, R., 1990: The thermocline as an ''internal boundary layer.'' *J. Mar. Res.,* **48,** 437–469.

Samelson, R., and G. K. Vallis, 1997a: A simple friction and diffusion scheme for planetary geostrophic basin models. *J. Phys. Oceanogr.,* **27,** 186–194.

——, and ——, 1997b: Large-scale circulation with small diapycnal diffusion: the two-thermocline limit. *J. Mar. Res.,* **55,** 223–275.

Stommel, H. and A. Arons, 1960: On the abyssal circulation of the world ocean—I. Stationary planetary flow patterns on a sphere. *Deep-Sea Res.,* **6,** 140–154.

Toole, J., R. Schmitt, K. Polzin, and E. Kunze, 1997: Fine and microstructure evidence of boundary mixing above the flanks of a mid-latitude seamount. *J. Geophys. Res.,* **102,** 947–959.

Welander, P., 1971: The thermocline problem. *Philos. Trans. Roy. Soc. London,* **270A,** 415–421.

Wesson, J., and M. Gregg, 1994: Mixing at Camarinal Sill in the Strait of Gibraltar. *J. Geophys. Res.,* **99,** 9847–9878.